Metabolomic and Lipidomic Alterations in Patients with Atopic Dermatitis with Dupilumab-Associated Ocular Surface Disease

VijayKumar Patra[1,2,7], Nora Woltsche[3,7], Natalie Bordag[1], Urban Cerpes[1], Danijela Bokanovic[1], Maria Repelnig[1], Yohann Clement[4], Isabella Perchthaler[1], Harald Köfeler[5], Manuela Fischl[3], Franz Legat[1], Andreas Wedrich[3], Jutta Horwath-Winter[3], Sophie Ayciriex[4] and Peter Wolf[1,6]

JID Innovations (2025);**5:**100361 doi:10.1016/j.xjidi.2025.100361

Atopic dermatitis (AD) is an inflammatory skin disease characterized by chronic pruritic eczema with an estimated prevalence of 10% in adults and 50% of them suffering from moderate-to-severe manifestations. Dupilumab, an IL-4/IL-13 inhibitor, is approved for treating moderate-to-severe AD. However, dupilumab-associated ocular surface disease (DAOSD) emerges in up to 60% of dupilumab-treated patients, constituting a major AD-specific adverse event. DAOSD pathogenesis has not been fully understood yet. To elucidate the metabolic changes occurring after dupilumab treatment in patients with AD, we focused in this prospective single-center cohort study particularly on patients who developed DAOSD. In total, 20 patients with AD underwent dupilumab therapy, with 6 developing DAOSD. Plasma and serum samples were collected at baseline, 4 and 16 weeks after treatment initiation, and during the conjunctivitis episode. In addition, 10 age- and sex-matched healthy controls were sampled solely at baseline. High-resolution mass spectrometry was employed for metabolomic and lipidomic analysis of all blood samples. Targeted metabolomics and lipidomic with multivariate analysis unveiled significant metabolic and lipidic disparities (such as increased activity of benzoic acid, tyrosine and indole metabolism, and others) between AD patients with and those without DAOSD. Metabolomics and lipidomic analysis further deepen our comprehension of DAOSD pathogenesis.

Keywords: Atopic dermatitis, Conjunctivitis, Dupilumab, Metabolomics, Plasma

INTRODUCTION

Atopic dermatitis (AD) is an inflammatory skin disease characterized by recurrent, localized, pruritic eczema with an estimated prevalence of up to 20% in children and 10% in adults, whereas about 20% of affected children and 50% of affected adults suffer from moderate-to-severe disease (Ständer, 2021; Weidinger and Novak, 2016). However, AD is not solely a skin pathology but may be regarded as a systemic disease because it also presents with various other organ manifestations (Darlenski et al, 2014). Metabolomics research has been an evolving field in recent years and allowed us to dive deeper in the pathophysiology of diseases. Intriguingly, patients with AD show significant metabolome alterations in serum, urine, sweat, skin, and feces compared with healthy individuals, and their metabolic profiles can change during treatment (Zhang et al, 2023, 2022). In the past, systemic treatment options for moderate-to-severe AD were limited by toxicity; thus, the introduction of dupilumab as the first biologic agent for the treatment of AD was revolutionary (Boguniewicz et al, 2017). Dupilumab, a human IgG4 mAb against IL-4 receptor α-subunit of IL-4 and IL-13, was approved in 2017 in the European Union for treatment of moderate-to-severe AD in adults (European Medicines Agency, 2023). Meanwhile, it has also been approved for children aged >6 months (European Medicines Agency, 2023). However, besides the great therapeutic success in significantly reducing cutaneous signs and symptoms, dupilumab has some side effects (European Medicines Agency, 2023). One adverse effect is dupilumab-associated ocular surface disease (DAOSD), which has been observed in a significant portion (20−30%) of adolescents and adults according to several clinical

[1]Department of Dermatology, Medical University of Graz, Graz, Austria; [2]Centre International de Recherche en Infectiologie, Institut National de la Santé et de la Recherche Médicale U1111, Centre National de la Recherche Scientifique, UMR5308, Ecole Normale Supérieure de Lyon, Université Claude Bernard Lyon 1, Université de Lyon, Lyon, France; [3]Department of Ophthalmology, Medical University of Graz, Graz, Austria; [4]Institut des Sciences Analytiques, CNRS UMR 5280, Université Claude Bernard Lyon 1, Université de Lyon, Villeurbanne, France; [5]Core Facility for Mass Spectrometry, Medical University of Graz, Graz, Austria; and [6]BioTechMed Graz, Graz, Austria

[7]These authors contributed equally to this work.

Correspondence: Vijaykumar Patra, Department of Dermatology, Medical University of Graz, Auenbruggerplatz 8, Graz 8036, Austria. E-mail: vijaykumar.patra@gmail.com and Peter Wolf, Department of Dermatology, Medical University of Graz, Auenbruggerplatz 8, Graz 8036, Austria. E-mail: Peter.wolf@medunigraz.at

Abbreviations: AD, atopic dermatitis; DAOSD, dupilumab-associated ocular surface disease; EASI, Eczema Area and Severity Index; PLS-DA, partial least-squares discriminant analysis

Received 13 August 2024; revised 16 February 2025; accepted 20 February 2025; accepted manuscript published online XXX; corrected proof published online XXX

Cite this article as: JID Innovations 2025;5:100361

studies (Kamata and Tada, 2021). The pathogenesis of DAOSD has not been fully understood yet. In a recent paper, Patra et al (2023) showed that DAOSD was characterized by persistent conjunctival neutrophil infiltration, a singular ocular surface microbial landscape, and elevated serum levels of certain proinflammatory cytokines. To take this further, we have now employed metabolomics that allows to phenotype the status of biological systems by quantifying (relative) molecules smaller than 1500 Da. Metabolites result from cellular metabolism and have a wide range of biological functions, including supporting cell growth, defense, inhibition, and stimulation of various cellular processes. In this study, we investigated the metabolome by metabolomic and lipidomic analyses in plasma and serum samples from the study cohort of Patra et al (2023) to elucidate the metabolic differences between patients with AD developing DAOSD and patients with AD not developing DAOSD.

RESULTS AND DISCUSSION

The study cohort from which the samples were obtained consisted of 20 adult patients with moderate-to-severe AD and 10 sex- and age-matched healthy controls (Patra et al, 2023). Six of 20 patients with AD had developed DAOSD in this study. Patients with AD had received a loading dose of 600 mg dupilumab and consecutive doses of 300 mg every second week for the entire study period of 16 weeks. In this study, we conducted a baseline visit before dupilumab initiation, a visit after 4 weeks of treatment, a final visit after 16 weeks of treatment, and an additional visit during the study, when an individual patient had developed DAOSD. At every visit, an ophthalmological slit-lamp examination; a dermatologic whole-body examination, including completion of Eczema Area and Severity Index (EASI) and Investigator's Global Assessment; and blood collection were performed (Patra et al, 2023). Detailed patient characteristics are provided in Table 1. The study described in this paper conformed to the principles of the Declaration of Helsinki. Informed consent was obtained from all study participants and controls. Approval was obtained from the Ethics Committee of the Medical University of Graz (ethical application number 31- 379 ex 18/19).

Clinical metabolomics, which is usually performed using serum or plasma samples, is an important tool to understand disease mechanisms and to monitor therapeutic response. However, the nature of sample collection and processing (serum is collected after blood coagulation) might alter the metabolome (Hagn et al, 2024; Yu et al, 2011); thus, we

Table 1. Demographic and clinical characteristics of AD patients with and without DAOSD

Characteristics	AD patients without DAOSD	AD patients with DAOSD	*P*-Value
Number of patients (count)	14	6	
Age, y, median (IQR [Q1–Q3])	38 (28–55)	37 (36–43)	.74
Sex (count)	M: 9; F: 5	M: 4; F: 2	NA
History of ocular surface disease (count)	6	3	>.99
Topical lubricants at baseline (count)	4	2	>.99
Visit 1 (baseline)			
Number of patients (count)	14	6	
EASI, median (IQR [Q1–Q3])	33.2 (20.2–42.5)	27.2 (18.4–38.3)	.43
IGA, median (IQR [Q1–Q3])	4 (3.7–4)	4 (3–4)	.58
BSA, median percentage (IQR [Q1–Q3])	78.7 (64.1–91.6)	77.6 (27.8–96.6)	.7
Head and neck, mean %	85.7	70.8	NA
Upper limbs (left; right), mean %	82.1; 82.1	70.8; 66.6	NA
Lower limbs (left; right), mean %	75; 71.4	66.6; 66.6	NA
Anterior trunk, mean %	76.7	62.5	NA
Back, mean %	73.2	62.5	NA
Genitals, mean %	1.7	29.1	NA
Visit 2 (1 mo after dupilumab)			
Number of patients (count)	11	5	
EASI, median (IQR [Q1–Q3])	13.9 (6.4–20.4)	14.6 (10.5–26)	.46
IGA, median (IQR [Q1–Q3])	3 (2-4)	3 (2–3.5)	.91
Visit DAOSD (at the time of ocular surface disease)			
Number of patients (count)	NA	6	NA
EASI, median (IQR [Q1–Q3])	NA	11 (5.97–20.93)	NA
IGA, median (IQR [Q1–Q3])	NA	3 (2–3)	NA
Time between visit 1 and visit DAOSD, d, median (range)	NA	53.5 (28–103)	NA
Visit 3 (4 mo after dupilumab)			
Number of patients (count)	12	6	
EASI, median (IQR [Q1–Q3])	8.5 (3.05–12.6)	10.9 (5.17–24.10)	.35
IGA, median (IQR [Q1–Q3])	2 (1.25–2)	3 (1.75–3.25)	.91

Abbreviations: AD, atopic dermatitis; BSA, body surface area; DAOSD, dupilumab-associated ocular surface disease; EASI, Eczema Area and Severity Index; F, female; IGA, Investigator's Global Assessment; IQR, interquartile range; M, male; NA, not applicable.

performed metabolomics analysis of both plasma and serum samples.

Plasma and serum samples were subjected to an untargeted metabolomic and lipidomic measurement using ultrahigh performance liquid chromatography coupled with mass spectrometry. The data analysis obtained 20 metabolites and 118 lipids, whereas the untargeted data retained a total of 7931 metabolic and lipidic features after data quality control. Part of the untargeted features were found only in plasma (1112) or only in serum (1593), resulting in a total of 6338 features in plasma and 6819 in serum for statistical analysis.

First, we compared the baseline global metabolomic profile of the control subjects with those of either patients with AD (no-DAOSD) or patients with AD who later developed DAOSD (Figure 1). We employed multivariate methods to compare the overall metabolome between different samples. Partial least-squares discriminant analysis (PLS-DA) is performed as one of a multivariate statistical method that identifies underlying patterns such as similarities of samples and differences between sample groups. The results are projected onto a 2-dimensional scores plot where each dot represents the metabolome of a sample quantified in that sample at baseline and proximity represents metabolic similarities. For each group, the 95% confidence interval is shown as ellipses. The PLS-DA method allowed us to focus on and enhance the group separations. Moreover, this method effectively highlighted metabolites differentiating between baseline levels of AD (no-DAOSD), DAOSD, and control samples.

In Figure 1a and b scores plots, each data point represents a sample's metabolic profile, with proximity indicating similarity and distance reflecting dissimilarity. The components 1 and 2 capture a significant portion of the total variance in the metabolic data (eg, 8.1 and 9.6% in Figure 1a), emphasizing the strength of the separation between groups. For better readability across plasma and serum, the x-axes of the plasma PLS-DA plots have been multiplied by −1, as indicated in the figures, because interpretation of the classification results is independent of direction. The 95% confidence ellipses further highlight the statistically significant differences between the groups.

To assess the predictive power of the model, a receiver operating characteristic analysis was conducted, evaluating the ability to correctly classify samples of one group versus all other groups on the basis of their metabolic profiles. With area under the curve values approaching 1, it is evident that

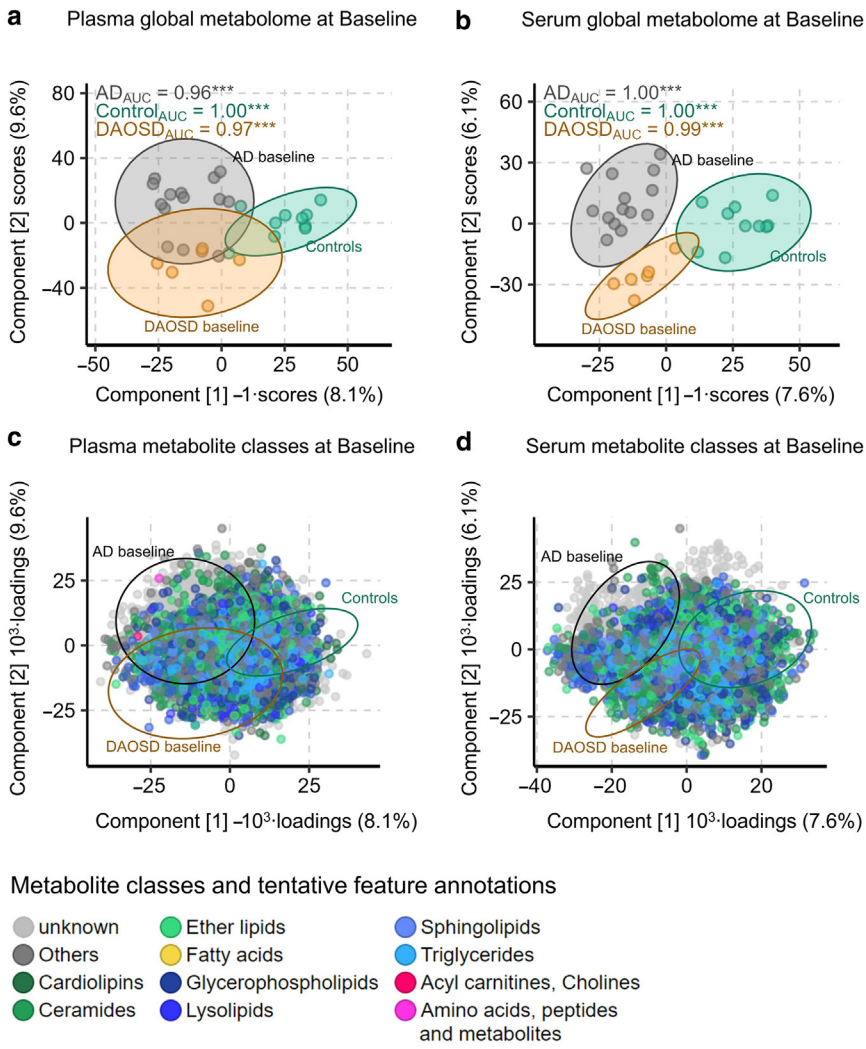

Figure 1. Metabolic profile of patients with DAOSD and AD at baseline. Presented is a supervised multivariate analysis with PLS-DA maximizing group differences. In the resulting scores plot of (**a, b**) plasma and serum at baseline, each subject's metabolome is represented, with proximity denoting similarity. The metabolomes of controls, patients with AD without DAOSD, and patients with AD who later developed DAOSD had already at baseline (prior to treatment) significantly differing metabolomes (n = 30). (**c, d**) The corresponding loadings plots represents the contribution of each feature to the group separation, which was in this case not driven by a single feature class. The ellipse represents 95% confidence interval. X-axes represent the (**a, b**) scores or (**c, d**) loadings of the first component. The Y-axis represent scores and loadings of the second component, also indicating the percentage of explained variability per component in parenthesis. AD, atopic dermatitis; AUC, area under the curve; DAOSD, dupilumab-associated ocular surface disease; PLS-DA, partial least squares discriminant analysis.

the model effectively discriminates between the 3 groups when leveraging the first 2 latent variables. This underlines the significant separation between the metabolic profiles of the different groups.

We observed significant differences in the metabolic profiles between the cohorts at baseline in plasma (Figure 1a) and serum (Figure 1b) samples as shown in PLS-DA score plots. In contrast to the sample representation, the loadings plot (Figure 1c and d) visualizes the contribution of each feature (metabolite) to the group separation observed in PLS-DA scores plot. The PLS-DA loading plot is crucial in interpreting the impact of each metabolite on the discriminant components. Features located farther from the origin contribute more to metabolic distinctions between groups. The position of a feature relative to the group in the scores plot reveals its upregulation in that group.

The corresponding loadings plots showed that these metabolic differences were driven by many various features encompassing all tentatively annotated lipid classes and many polar unknowns.

Moreover, we have used univariate methods to compare the differences at a level of single metabolites between groups independently of all other metabolites. NLME (nonlinear mixed-effects model) is a statistical method such as ANOVA that is able to handle repeated measures, heterogeneous intragroup variances, and non-normal distributions to assess the differences between groups. The group differences are represented by contrast ratios of pairwise comparison and shown in the plot as a triangle in the direction of the change for each feature (Figure 2a and b). Red and blue numbers indicate the total number of significantly upregulated or downregulated features in that pairwise comparison. The gray frame indicates the increase of significantly changed features with progressing treatment time.

We observed several significant up or downregulated features at baseline when compared between AD (no-DAOSD) and control, DAOSD and control, and AD (no-DAOSD) and DAOSD, suggesting a strong difference at the metabolic profiles at the baseline both in plasma and serum (Figure 2a and b). Furthermore, feature changes were used for a mummichog-based prediction of pathway activity utilizing metabolic networks bypassing annotation of untargeted features, which revealed several notably impacted pathways such as glycosyldiradylglycerols, glycerophosphoinositols, glycerophosphoethanolamines, phosphatidylcholine, and phosphosphingolipids, and more were downregulated in DAOSD than in AD (no-DAOSD), both in plasma and serum (normalized enrichment score < 3, $P < .05$) (Figure 2c). Numerous metabolic pathways were significantly lower in patients with DAOSD at baseline than in control subjects (Figure 2c). These results strongly indicate that several metabolic pathways in patients with DAOSD are already at an altered state before initiation of dupilumab treatment. Interestingly, a recent study revealed several inflammatory mediators to be different between patients with AD (no-DAOSD) and those with DAOSD (Thormann et al, 2024). Among these preexisting metabolic features and/or pathways, inflammatory mediators could serve as a diagnostic criterion for patients with AD who will be subjected to dupilumab treatment in predicting DAOSD.

Furthermore, the comparison of patients with AD (no-DAOSD) or DAOSD to healthy controls with univariate analysis found 9−14% of all features being significantly up or downregulated, underlining the strong metabolic impact of untreated disease (Figure 3a and b and Supplementary Data S1). Comparing patients after 4 weeks of dupilumab treatment with their respective baseline value revealed that metabolite profiles started to shift with an emphasis on downregulation. This trend intensified after 16 weeks and was similar between plasma and serum but less well-evident in patients with DAOSD.

The total number of significant features among various pairwise comparisons are summarized as bar charts for plasma and serum samples (Figure 4a and b). About 55% of all detected features were not impacted at all, and overlap of significant features was comparatively small, with only ∼1.5% being significantly regulated in more than 4 of the 7 regarded pairwise comparisons in plasma (Figure 4a). The overlap was slightly higher in serum with ∼3% of all features, whereas 60% of the features did not change at all (Figure 4b). Concentrating on features that were significant in at least 4 of the 7 pairwise comparisons revealed that most features were inversely fostered in untreated disease than in healthy controls and diminished after treatment initiation and vice versa (Figures 5 and 6). Thus, dupilumab drives a normalization of the metabolic profiles in a similar way for both plasma and serum. The metabolic normalization intensified in the course of the treatment over time and was often more pronounced in patients with DAOSD than in patients with AD (no-DAOSD).

These dynamic changes of metabolic features posed the question of whether various pathways are also differentially regulated in patients with AD (no-DAOSD) or DAOSD during the treatment. Many pathways were significantly enhanced in patients with DAOSD while remaining unchanged or only slightly decreased in patients with AD (no-DAOSD) for the same comparisons (Figure 7). The most prominently upregulated pathways in patients with DAOSD involved, for example, benzoic acids, citrulline biosynthesis, D-amino acid metabolism, proline biosynthesis, and arginine degradation VI pathway, especially 4 weeks after treatment initiation (Figure 7) versus baseline, as measured in plasma. Furthermore, at the time of the DAOSD episode, pathways such as tyrosine metabolism, indole metabolism, glyoxylate and dicarboxylate metabolism, NAD biosynthesis from 2-amino-3-carboxymuconate semialdehyde, and L-glutamine biosynthesis II were significantly enriched among few others compared with those at baseline (Figures 7 and 8).

Taken together, our results indicate that dupilumab induces significant changes in plasma and serum metabolic features and their associated pathways in patients with AD (no-DAOSD), which might be involved in DAOSD pathogenesis. Circulating metabolites, notably certain amino acids, have been linked with allergic conjunctivitis (Zou et al, 2024). In this study, we report that after 4 weeks of dupilumab treatment, patients with AD developing DAOSD have in particular increased metabolic activity of benzoic acids, which upon prolonged exposure or accumulation may lead to severe irritation on the ocular surface and cause inflammation and conjunctivitis (Aguilar et al, 2016). Free citrulline

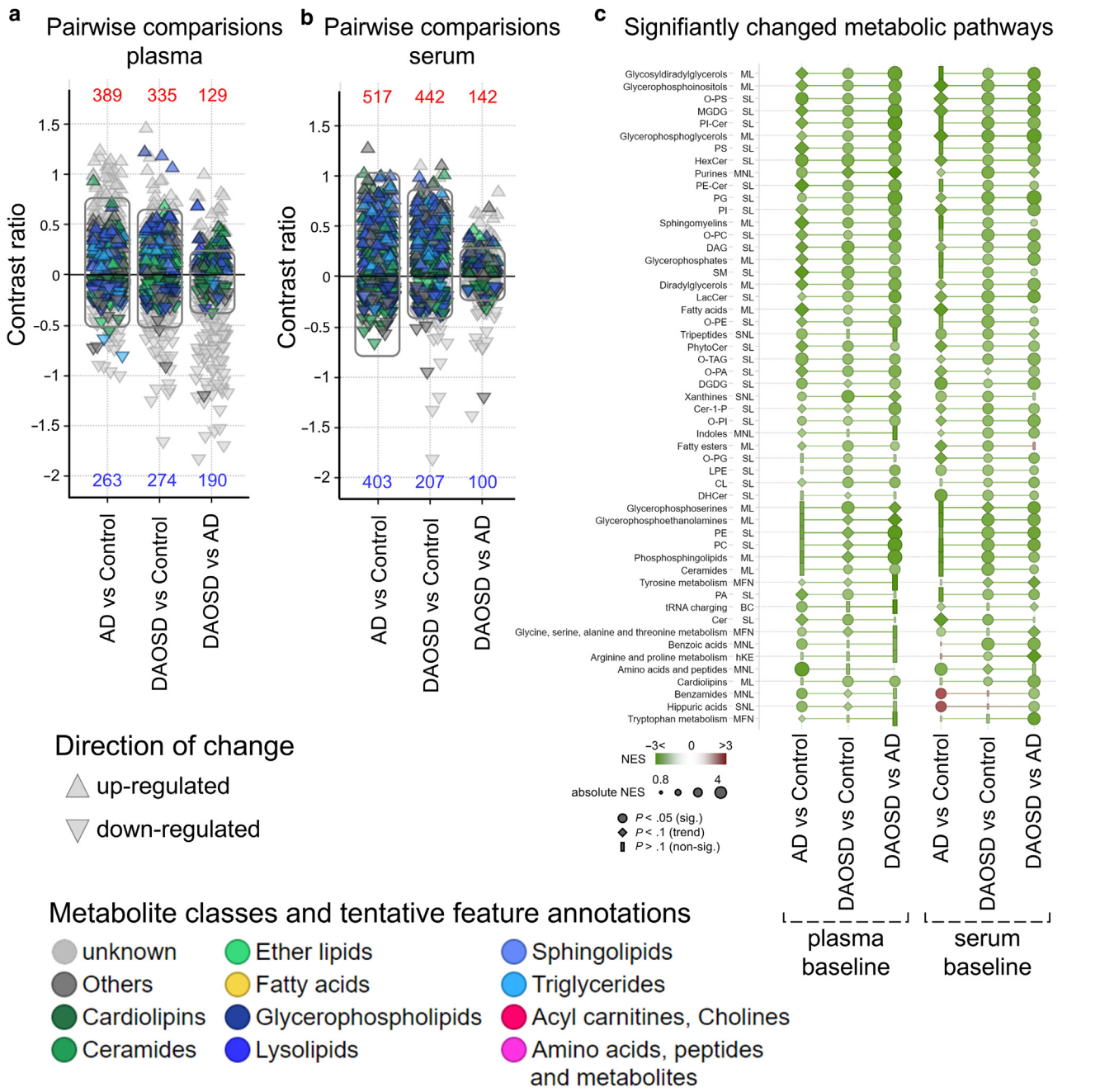

Figure 2. Metabolic differences at baseline. Shown are univariate analysis results per feature and investigated pairwise comparisons (at baseline) showing each features' contrast ratio. Labels represent total numbers of significantly ($P < .05$) up (red) and downregulated (blue) features, which are colored by class as in (**a, b**) plasma and serum. The gray frame represents the total number of significantly up/downregulated feature. All analysis were based on log_{10}-transformed data. (**c**) NESs encoding the strength and direction of the impacted pathway in both plasma and serum at baseline between different groups. Pathway analysis results are color coded by their NESs, which encode the strength and direction of the metabolic impact in each pairwise comparison. Pathways are sorted by the descending number of significantly changed pathways and summed absolute NES over all pairwise comparisons. Owing to space constraints, only pathways with results in all pairwise comparisons and a total summed NES ≥10 are shown, and the pathway's libraries were abbreviated (details are provided in Materials and Methods). $P < .05$ (significant) and $P > .05$ (nonsignificant). NES, normalized enrichment score.

circulating in the blood is formed by catabolism of amino acids and during the production of nitric oxide, which is then converted to arginine that is known to be involved in allergic conjunctivitis (Meijer et al, 1996). Furthermore, previous research has shown that L-citrulline and proline-rich proteins are involved in interactions with the ocular surface microbiome (Zysset-Burri et al, 2021). We have previously shown that a unique ocular surface microbiome exists in patients with DAOSD (Patra et al, 2023). Considering this study's new data, we hypothesize that an altered ocular surface microbiome might be associated with citrulline and proline metabolism, leading to DAOSD.

At the time of DAOSD, we also observed increased tyrosine activity, which in high levels is known to be associated

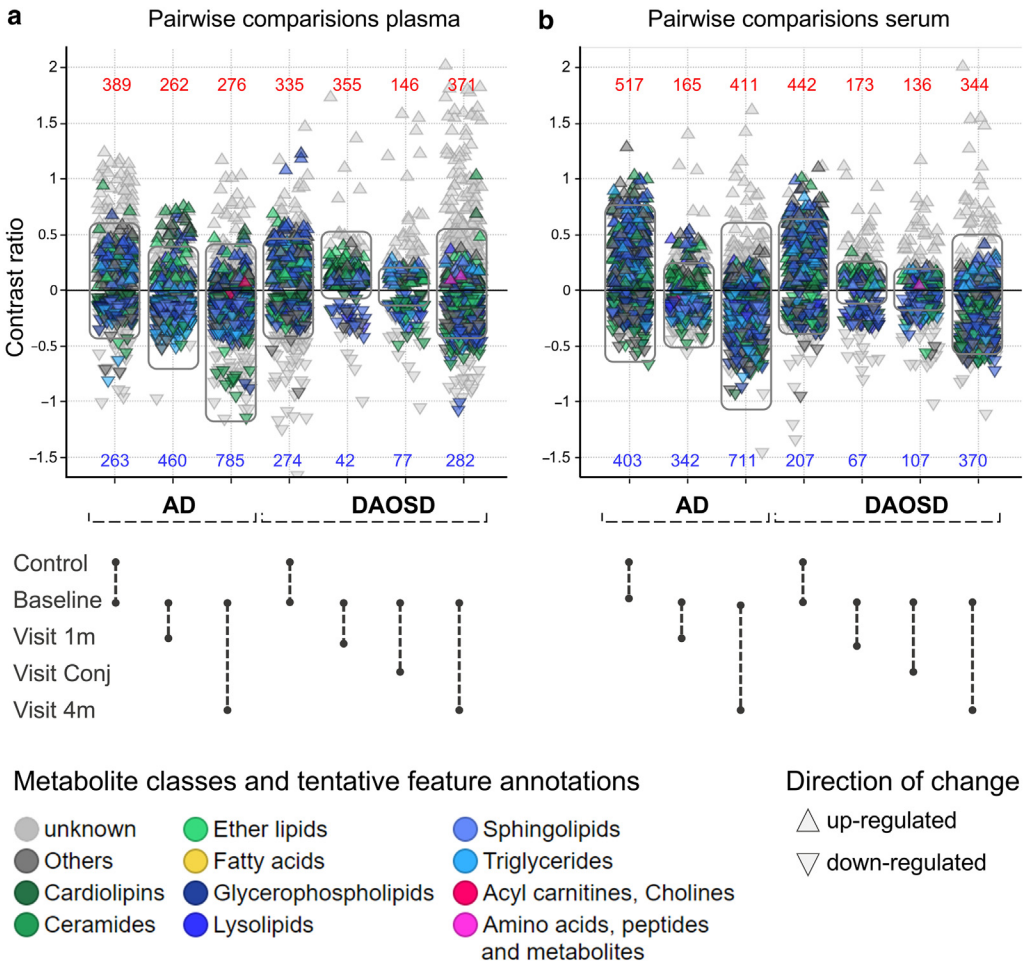

Figure 3. Metabolic differences between groups with treatment progression. (**a, b**) Univariate analysis results per feature and investigated pairwise comparisons (compared groups indicated dumbbells below) showing each features' contrast ratio in plasma and serum. Labels represent total numbers of significantly ($P < .05$) up (red) and downregulated (blue) features, which are colored by class. The gray frame represents the total number of significantly up/downregulated feature. All analysis were based on log_{10}-transformed data. Visit 1m denotes visit at 1 month, Visit Conj denotes visit during conjunctival episode, and Visit 4m denotes visit at 4 months.

with skin and conjunctivital lesions (Aydin et al, 2003). Metabolic pathways related to glyoxylate and dicarboxylate metabolism, which are known to be associated with the conjunctival microbiome (Zhu et al, 2021), as well as NAD biosynthesis from 2-amino-3-carboxymuconate semi-aldehyde (Navarro et al, 2022) and L-glutamine biosynthesis II (Song et al, 2023), which help regulate regulate immune responses and are associated to allergic conjunctivitis (Zou et al, 2024), were all increased in patients with DAOSD.

We performed linear correlation analysis of all the metabolic features and clinical data (EASI and neutrophil counts in ocular surface H&E) at all available time points (baseline, visit

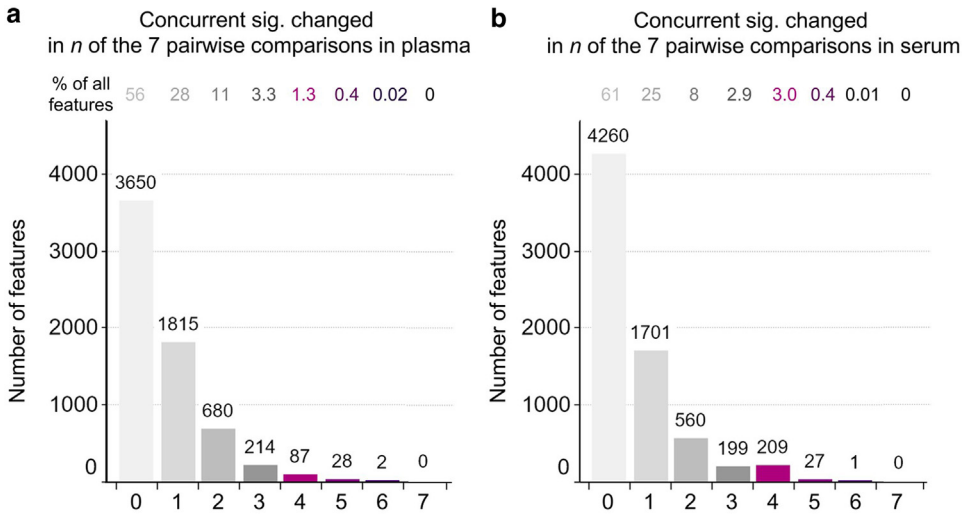

Figure 4. Number of metabolic features concurrently changed. Bar chart of how many features were significant (denoted as sig) concurrently in how many of the 7 pairwise comparisons from Figure 3 in either (**a**) plasma or (**b**) serum.

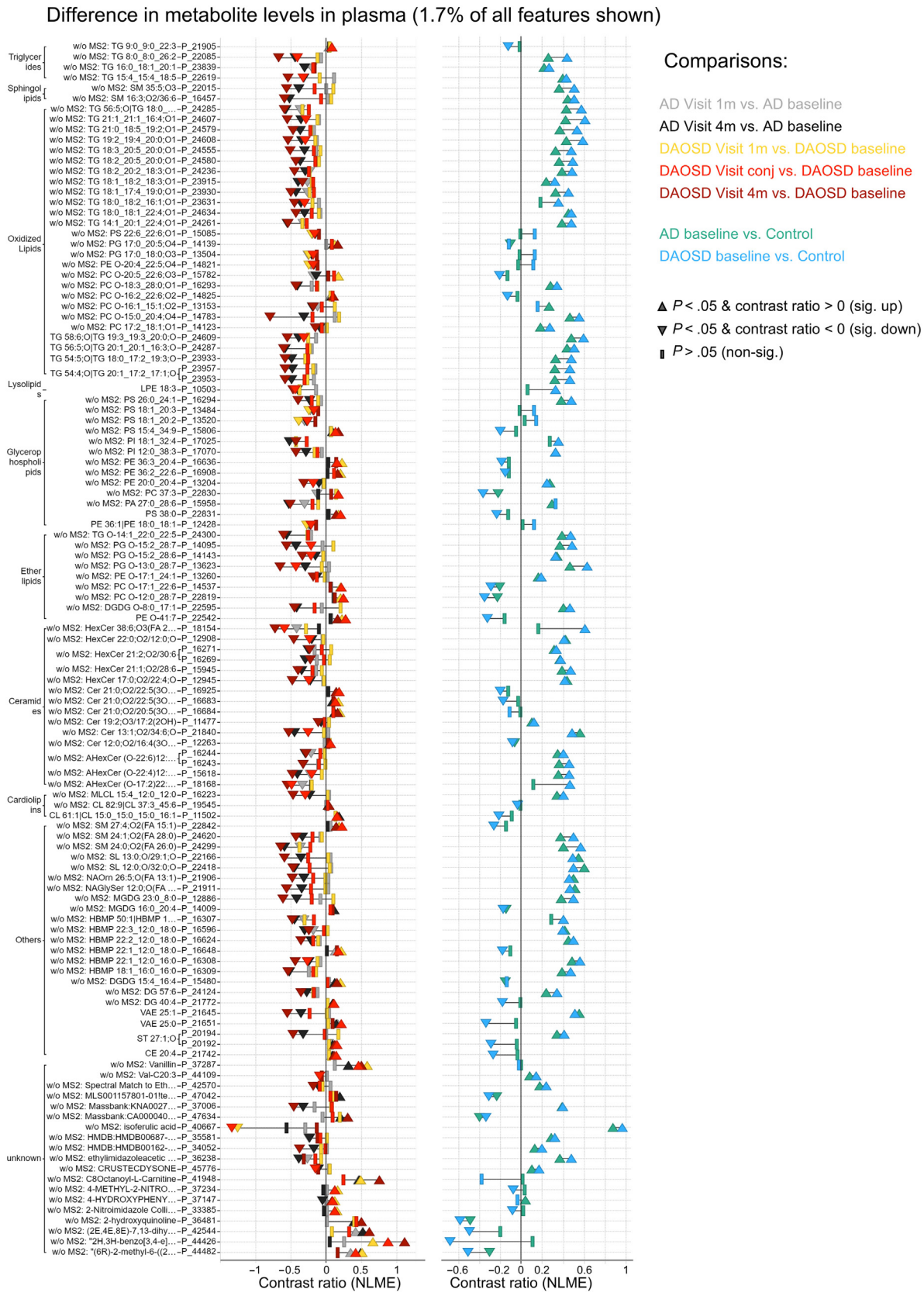

Figure 5. Specific plasma metabolic features are intensified in patients with DAOSD. (**a**) Dumbbell plot of all features significant in at least 4 of the 7 pairwise comparisons (color coded) from Figure 3 in plasma samples. The plot shows the strength of metabolic changes along the x-axis, feature names along the y-axis, and significance encoded in shapes ($P < .05$). Visit 1m denotes visit at 1 month, Visit Conj denotes visit during conjunctival episode, and Visit 4m denotes visit at 4 months. AD, atopic dermatitis; DAOSD, dupilumab-associated ocular surface disease; NLME, nonlinear mixed effect.

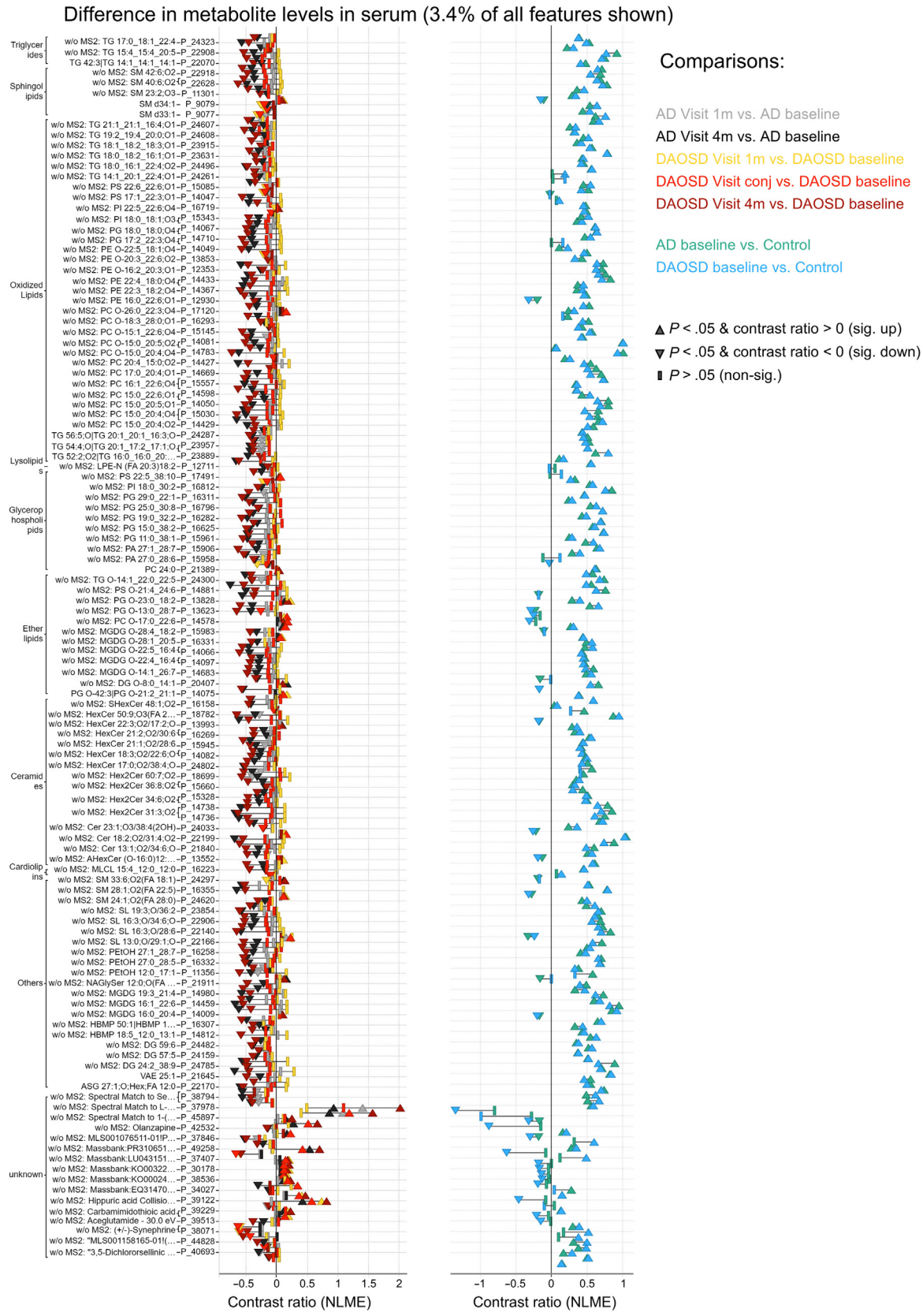

Figure 6. Specific serum metabolic features are intensified in patients with DAOSD. (**a**) Dumbbell plot of all features significant in at least 4 of the 7 pairwise comparisons (color coded) from Figure 3 in serum samples. The plot shows the strength of metabolic changes along the x-axis, feature names along the y-axis, and significance encoded in shapes ($P < .05$). Visit 1m denotes visit at 1 month, Visit Conj denotes visit during conjunctival episode, and Visit 4m denotes visit at 4 months. DAOSD, dupilumab-associated ocular surface disease; NLME, nonlinear mixed effect.

Figure 7. Metabolic pathways upregulated in patients with DAOSD in contrast to those in patients with AD. (**a**) Bar plot of how many pathways were significant (denoted as sig) in how many of the 7 pairwise comparisons from Figure 3. (**b**) Pathway analysis results are color coded by their NES, which encodes the strength and direction of the metabolic impact in each pairwise comparison. Pathways are sorted by the descending number of significantly changed pathways and summed absolute NES over all pairwise comparisons. Owing to space constraints, only pathways with results in all pairwise comparisons and a

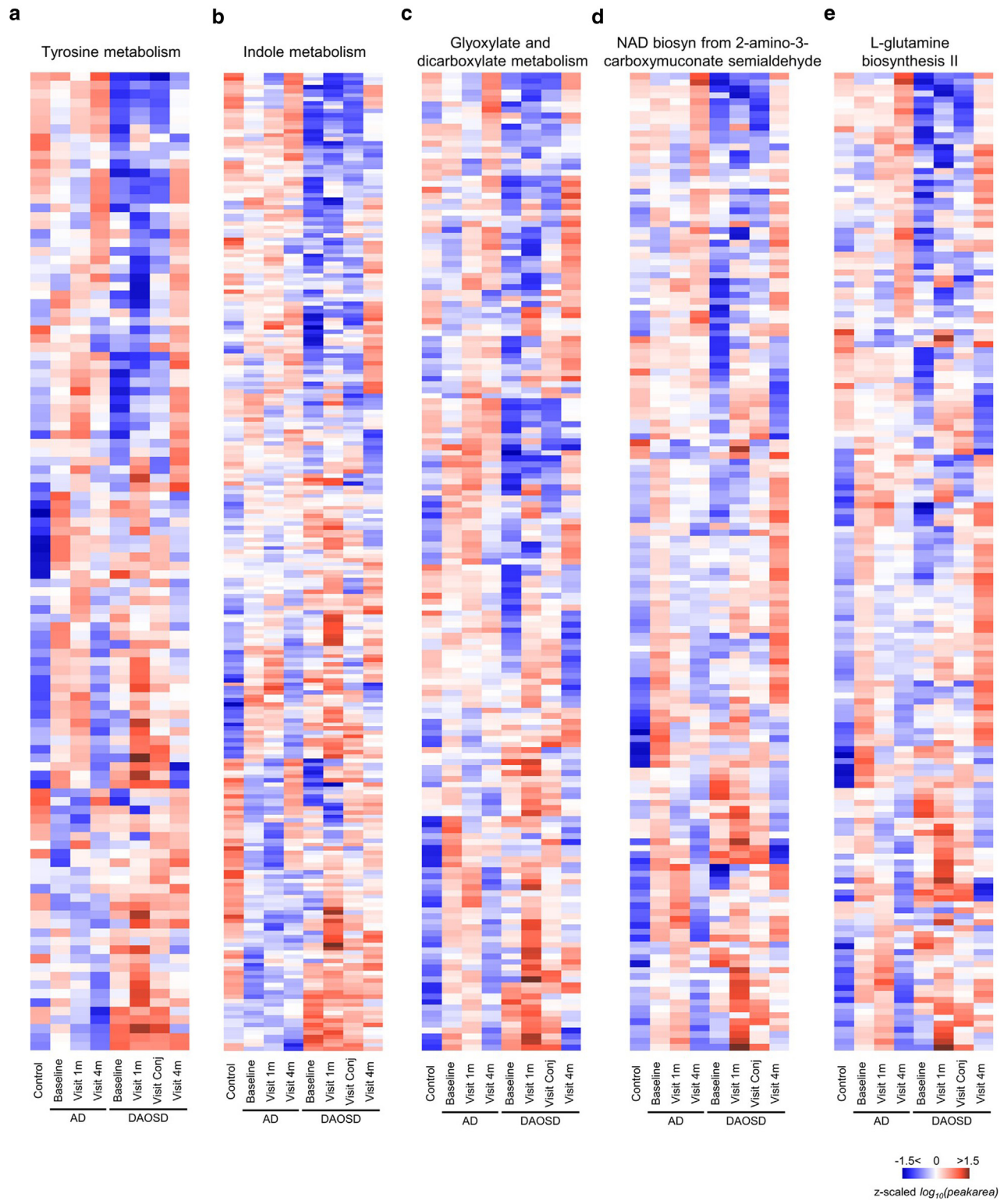

Figure 8. Feature levels of selected pathways visualized as heatmaps. The z-scaled, log_{10}-transformed peak areas were averaged per group. Each heatmap shows all features that were matched to the pathway (**a**) tyrosine metabolism, (**b**) indole metabolism, (**c**) glyoxylate and dicarboxylate metabolism, (**d**) NAD biosynthesis from 2-amino-3- carboxymuconate semialdehyde, and (**e**) L-glutamine biosynthesis II during mummichog-based prediction of pathway activity and are thus contributing to the metabolic networks when bypassing annotation of untargeted features. AD, atopic dermatitis; DAOSD, dupilumab-associated ocular surface disease.

total summed NES ≥19 are shown, and the pathway's libraries were abbreviated (details are provided in Materials and Methods). $P < .05$ (significant) and $P < .1$ (trend) and $P > .1$ (nonsignificant). AD, atopic dermatitis; DAOSD, dupilumab-associated ocular surface disease; NES, normalized enrichment score.

at 1 month, visit during conjunctival episode, and visit at 4 months). As an example, the 4 strongest positive linear correlations against EASI are shown (Figure 9a). The results show that the correlations are independent of patient group or time points investigated. To gain mechanistic insight, we performed pathway analysis on the basis of the linear correlation results. In plasma, 36 pathways were significantly corelated with EASI or neutrophil counts (Figure 9b). These results suggest that high EASI is positively corelated, for example, with increased leukotriene biosynthesis pathway (Chari et al, 2001) and a precursor pathway such as biosynthesis of unsaturated fatty acids. Neutrophil counts (ocular surface H&E) are positively correlated with metabolic pathways such as benzenesulfonyl compounds and P-methoxybenzoic acids. Interestingly, in patients with DAOSD, the benzoic acid pathway is significantly upregulated 1 month after dupilumab initiation.

In an analog approach, we also performed linear correlation analysis of all metabolic features against all blood results at all available time points (baseline, visit 4) followed by pathway analysis (Figure 10). As expected, these results showed high correlation of kidney markers such urea and creatinine, with amino acid degradation pathways (Brosnan and Brosnan, 2010), thus validating this analysis approach. We observed a positive correlation between inflammatory lipid mediator pathways (Serhan et al, 2008) including hydroxyeicosapentaenoic acid, leukotriene biosynthesis, leukotrienes, docosanoids, hydroxyeicosatetraenoic acid, and hydroxyeicosatrienoic acid - and precursors pathways such as biosynthesis of unsaturated fatty acids with blood levels of leukocytes and neutrophils.

In conclusion, our data reveal, to our knowledge, previously unreported insights into the systemic metabolic activity

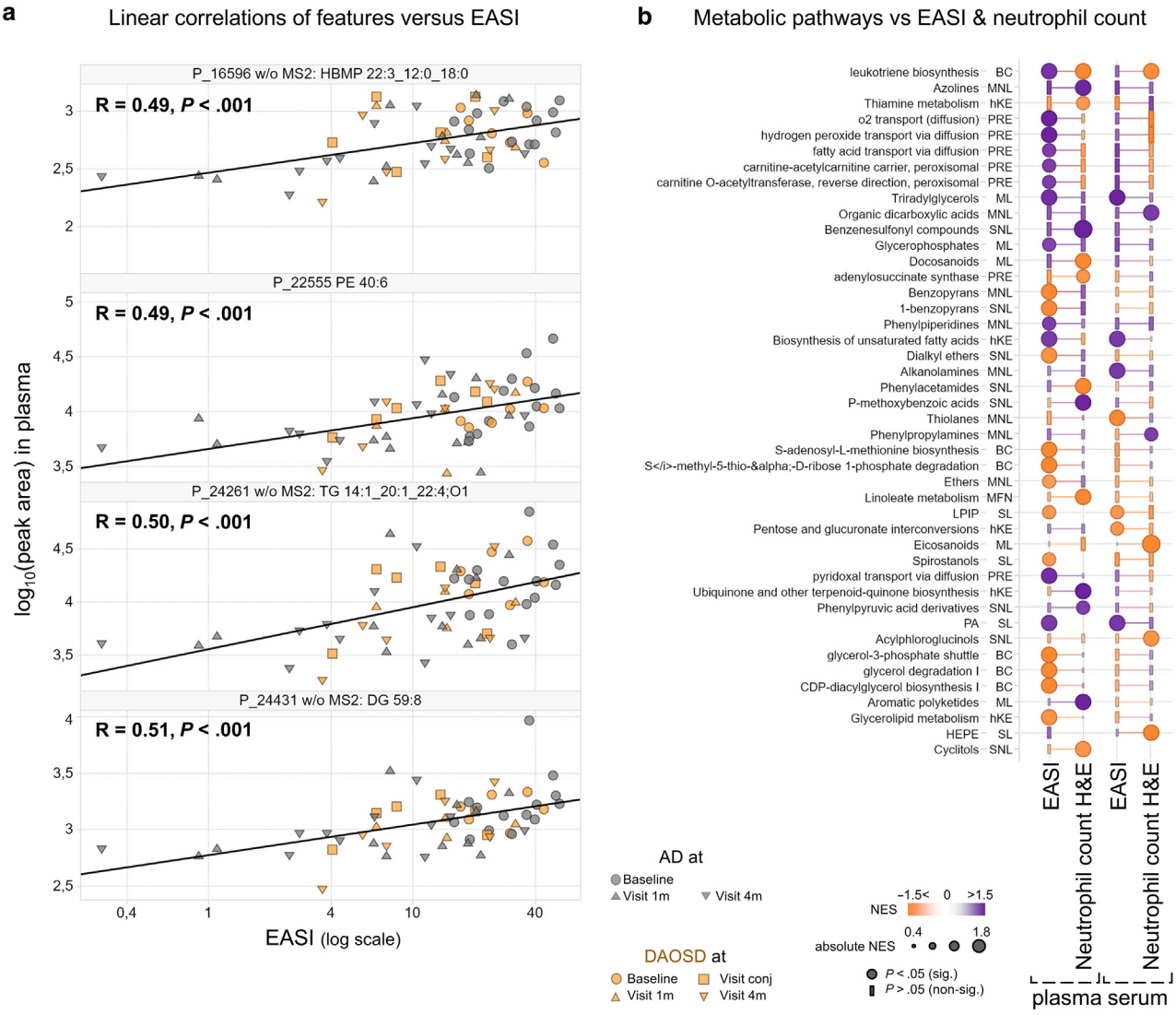

Figure 9. Metabolic pathways correlate with EASI and neutrophil counts in ocular surface. (**a**) Linear correlations were calculated for all features at all available time points (baseline, visit at 1 month, visit during conjunctival episode, and visit at 4 months). The 4 features with the strongest positive correlating to EASI are shown as an example. (**b**) Pathway analysis results based on these linear correlations are color coded by their NES, which encodes the strength and direction of the metabolic correlations. Pathways are sorted by the descending number of significantly changed pathways and summed absolute NES over all pairwise comparisons, showing only significantly correlating pathways. The pathway's libraries were abbreviated (details are provided in Materials and Methods). $P < .05$ (significant) and $P > .05$ (nonsignificant). Visit 1m denotes visit at 1 month, Visit Conj denotes visit during conjunctival episode, and Visit 4m denotes visit at 4 months. EASI, Eczema Area and Severity Index; NES, normalized enrichment score.

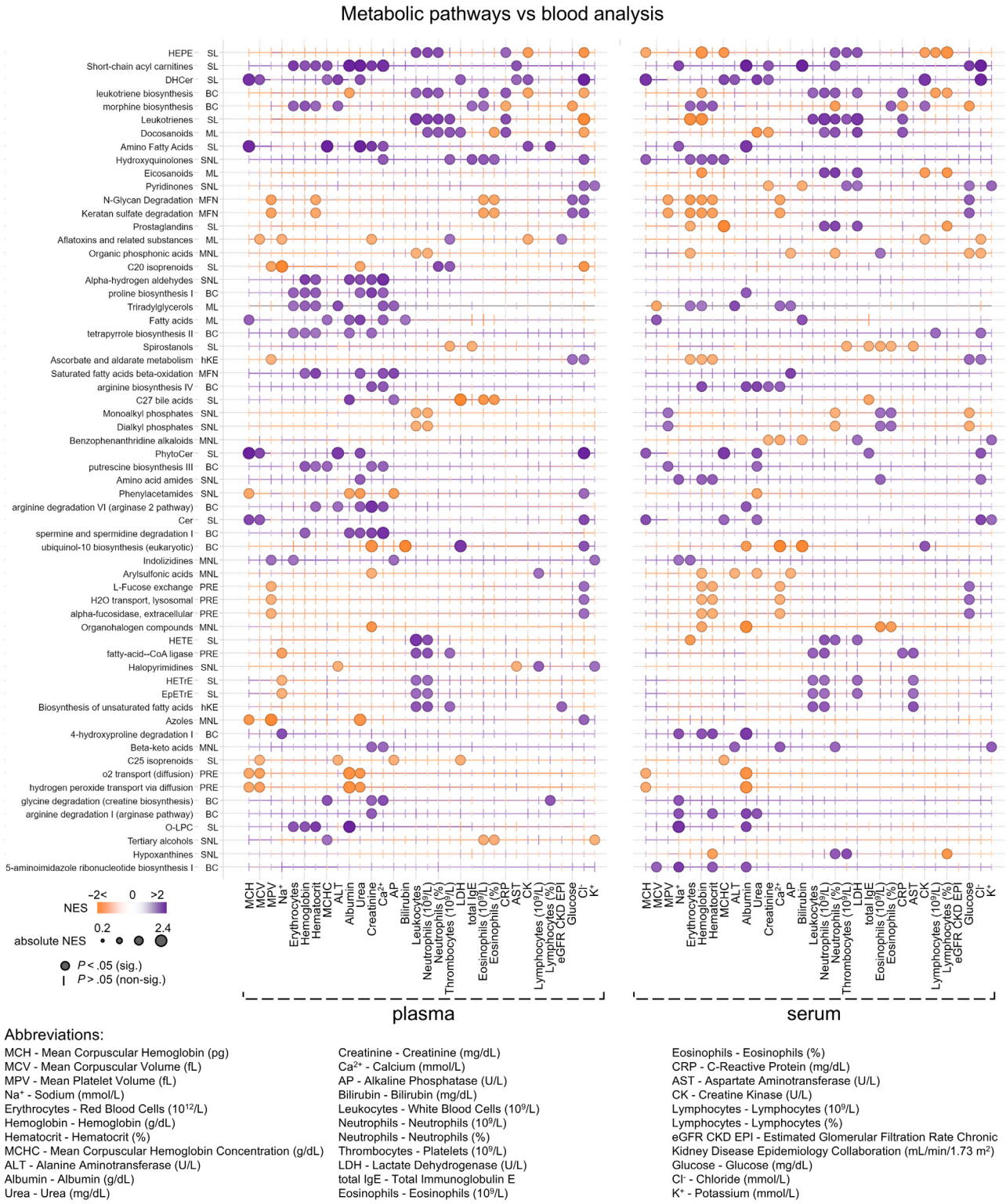

Abbreviations:

MCH - Mean Corpuscular Hemoglobin (pg)
MCV - Mean Corpuscular Volume (fL)
MPV - Mean Platelet Volume (fL)
Na^+ - Sodium (mmol/L)
Erythrocytes - Red Blood Cells (10^{12}/L)
Hemoglobin - Hemoglobin (g/dL)
Hematocrit - Hematocrit (%)
MCHC - Mean Corpuscular Hemoglobin Concentration (g/dL)
ALT - Alanine Aminotransferase (U/L)
Albumin - Albumin (g/dL)
Urea - Urea (mg/dL)
Creatinine - Creatinine (mg/dL)
Ca^{2+} - Calcium (mmol/L)
AP - Alkaline Phosphatase (U/L)
Bilirubin - Bilirubin (mg/dL)
Leukocytes - White Blood Cells (10^9/L)
Neutrophils - Neutrophils (10^9/L)
Neutrophils - Neutrophils (%)
Thrombocytes - Platelets (10^9/L)
LDH - Lactate Dehydrogenase (U/L)
total IgE - Total Immunoglobulin E
Eosinophils - Eosinophils (10^9/L)
Eosinophils - Eosinophils (%)
CRP - C-Reactive Protein (mg/dL)
AST - Aspartate Aminotransferase (U/L)
CK - Creatine Kinase (U/L)
Lymphocytes - Lymphocytes (10^9/L)
Lymphocytes - Lymphocytes (%)
eGFR CKD EPI - Estimated Glomerular Filtration Rate Chronic Kidney Disease Epidemiology Collaboration (mL/min/1.73 m^2)
Glucose - Glucose (mg/dL)
Cl^- - Chloride (mmol/L)
K^+ - Potassium (mmol/L)

Figure 10. Metabolic pathways correlate with blood results. Linear correlations were calculated for all features at all available time points (baseline, visit 4) against all numeric blood results with >15 values. Pathway analysis results based on these linear correlations are color coded by their NES, which encodes the strength and direction of the metabolic correlations. Pathways are sorted by the descending number of significantly changed pathways and summed absolute NES over all pairwise comparisons. Owing to space constraints, only pathways significant in at least 4 correlations in either plasma or serum are shown, and the pathway's libraries were abbreviated (details are provided in Materials and Methods). $P < .05$ (significant) and $P > .05$ (nonsignificant). NES, normalized enrichment score.

in patients with AD who develop DAOSD. A recent study revealed several inflammatory mediators to be different between AD patients with and those without DAOSD (Thormann et al, 2024). These preexisting metabolic features, pathways, and inflammatory mediators can serve as a diagnostic criterion for patients with AD who will be subjected to

dupilumab treatment in predicting DAOSD. Although the results of this study need to be substantiated by larger cohorts and in vivo models, there is strong evidence that there is an established metabolic difference between AD patients with DAOSD and those without DAOSD, which is further altered after dupilumab treatment. These metabolic shifts could impact the ocular surface microbiome and inflammation leading to DAOSD.

MATERIALS AND METHODS

Patient characteristics

This study involved patients aged >18 years with moderate-to-severe AD who were scheduled for treatment with dupilumab (Patra et al, 2023). Detailed characteristics are provided in Table 1. Exclusion criteria included allergy to 0.4% oxybuprocaine hydrochloride eye drops (used for topical ocular anesthesia), pre-existing eye disease (such as glaucoma) requiring regular use of eye drops (other than artificial tear drops), active microbial inflammation of the ocular surface or allergic conjunctivitis at baseline, patients wearing contact lenses, and patients who have undergone ocular surgery in the last 6 months. Written, informed consent was obtained from all study participants and controls. This study was conducted according to the principles of the Declaration of Helsinki.

Clinical diagnosis of DAOSD

A thorough slit-lamp examination by the same ophthalmologist (NW) was performed at every visit. DAOSD was defined as previously reported as conjunctivitis, blepharitis (often combined as blepharoconjunctivitis), and/or keratitis. Conjunctivitis was defined as follicular or papillary conjunctivitis presenting with conjunctival injection, serous or mucous secretion accompanied by burning, foreign body sensation, itching (Utine et al, 2021). Blepharitis was defined as anterior blepharitis presenting with eyelid erythema, swelling, or desquamation or as posterior blepharitis presenting as meibomian gland dysfunction (Utine et al, 2021). Keratitis associated with DAOSD was defined as superficial (punctate) keratitis (Utine et al, 2021), limbitis presenting as Trantas' dots (Maudinet et al, 2019), or corneal infiltrate or ulcer (Phylactou et al, 2022), according to previous reports.

Clinical dermatological scoring

The EASI and Investigator's Global Assessment scoring was performed at each visit of every patient by dermatologists (UC, DB, and MR). These well-established scores quantify the severity of the diseases with a ranking from 0 to 72 for EASI and 0 to 4 for Investigator's Global Assessment.

Lipidomics

Our study used the same lipidomics and metabolomics methods that have been previously developed (Triebl et al, 2017) and used in various other publications (Zandl-Lang et al, 2022; Zhang et al, 2021; Zullig et al, 2020). To ensure consistency and reproducibility and improve the comprehensibility of the current results, the method description was retained.

Lipid extraction was carried out from 50 µl human serum or plasma according to a modified version of the original extraction protocol published by Matyash et al (2008). Methanol (1.5 ml) and methyl-tert-butyl ether (5 ml) were added to the samples in Pyrex glass tubes with teflon lined caps. After vortexing for 10 seconds, the mixture was incubated in an ice-cooled ultrasound bath for 10 minutes and were shaken in an overhead shaker for 10 minutes at room temperature. After addition of 1.25 ml deionized water and 10 minutes of additional overhead shaking, the mixture was centrifuged for 10 minutes at 1350*g* (room temperature), and the upper phase was transferred to a new glass tube. The lower phase was re-extracted with 2 ml of the upper phase of methyl-tert-butyl ether/methanol/deionized water (10:3:2.5, v/v/v), and again, the upper phase was collected and combined with the upper phase from the first extraction. Finally, the upper phase was evaporated in a vacuum centrifuge (Thermo Fisher Scientific) and dissolved in 500 µl chloroform/methanol (1:1, v/v). For negative measurement, 90 µl aliquots were spiked with 86.3 µl internal standards (chloroform/methanol, 1:1, v/v) containing 12:0/13:0 phosphatidylinositol, 17:0/20:4 phosphatidylinositol, 14:1/17:0 phosphatidylinositol, 21:0/22:6 phosphatidylinositol, 12:0/13:0 phosphatidylglycerol, 17:0/20:4 phosphatidylglycerol, 14:1/17:0 phosphatidylglycerol, 21:0/22:6 phosphatidylglycerol (1.5 µM each), and CL-Mix LM 6003 (2.4 µM). The solvent was evaporated under a gentle stream of nitrogen, and the sample was reconstituted in the same volume of injection solvent isopropanol/chloroform/methanol (90:5:5, v/v/v). For positive measurement 2.1 µl aliquots were spiked with 127.7 µl internal standards (chloroform/methanol, 1:1, v/v) containing phosphatidylcholine 12:0/13:0, phosphatidylcholine 17:0/20:4, phosphatidylcholine 14:1/17:0, phosphatidylcholine 21:0/22:6 (1 µM each), phosphatidylethanolamine 12:0/13:0, phosphatidylethanolamine 17:0/20:4, phosphatidylethanolamine 14:1/17:0, phosphatidylethanolamine 21:0/22:6, phosphatidylserine 12:0/13:0, phosphatidylserine 17:0/20:4, phosphatidylserine 14:1/17:0, phosphatidylserine 21:0/22:6 (1.5 µM each), TG-Mix LM 6000 (4 µM), lysophosphatidylcholine 17:1 (1 µM), SL-Mix LM6002 (1.5 µM each), cholesterol ester 19:0 (12 µM), and cholesterol-d7 (80 µM), and 36 µl of this mixture was used for further processing. The solvent was evaporated under a gentle stream of nitrogen, and the sample was reconstituted in 90 µl injection solvent isopropanol/chloroform/methanol (90:5:5, v/v/v).

Chromatographic separation for sphingolipids was performed as previously described in Triebl et al (2017). Briefly, chromatographic separation was performed on a Waters BEH C8 column (100 × 1 mm, 1.7 µm), thermostatted to 50 °C in a Dionex Ultimate 3000 RS ultrahigh-performance liquid chromatography system. Mobile phase A was deionized water containing 1 vol% of 1 M aqueous ammonium formate (final concentration of 10 mmol/l) and 0.1 vol% of formic acid as additives. Mobile phase B was a mixture of acetonitrile/isopropanol 5:2 (v/v) with the same additives. Gradient elution started at 50% mobile phase B, increasing to 100% B over 15 minutes; 100% B were held for 10 minutes, and the column was re-equilibrated with 50% B for 8 minutes before the next injection. The flow rate was 150 µl/minute, the samples were kept at 8 °C, and the injection volume was 2 µl.

The Orbitrap Velos Pro hybrid mass spectrometer (Thermo Fisher Scientific) was operated in data-dependent acquisition. Every sample was acquired once in positive polarity and once in negative using a HESI II ion source. Ion source parameters for positive polarity were as follows: source voltage of 4.5 kV, source temperature of 275 °C, sheath gas of 25 arbitrary units, aux gas of 9 arbitrary units, sweep gas of 0 arbitrary units, and capillary temperature of 300 °C. Ion source parameters for negative polarity were as follows: source voltage of 3.8 kV, source temperature of 325 °C, sheath gas of 30 arbitrary units, aux gas of 10 arbitrary units, sweep gas of 0 arbitrary units, and capillary temperature of 300 °C. Automatic gain control target value was set to 10^6 ions to enter the mass analyzer, with a maximum ion accumulation time of 500 ms. Full scan profile spectra from m/z 320 to 1050 for

positive ion mode and from 350 to 1600 in negative ion mode were acquired in the Orbitrap mass analyzer at a resolution setting of 100,000 at m/z 400. For tandem mass spectrometry experiments in positive and negative ion mode, the 10 most abundant ions (top 10) of the full scan spectrum were sequentially fragmented in the ion trap using He as collision gas (Collision-Induced Dissociation, normalized collision energy: 50, isolation width: 1.5, activation Q: 0.2, activation time: 10), and centroid product spectra at normal scan rate (33 kDa/s) were collected.

Liquid chromatography-tandem mass spectrometry data were processed using Lipid Data Analyzer (Hartler et al, 2017, 2011). Briefly, the algorithm identifies lipids with a 3-dimensional algorithm, using the 3 dimensions m/z, retention time, and intensity to correctly integrate peaks, while also considering the isotopic distribution. Tandem mass spectrometry spectra are considered for confirmation of structures by characteristic head group and fatty acyl fragments. Lipids are annotated according to the official international shorthand nomenclature (Liebisch et al, 2013).

Metabolomics

Sample preparation was performed according to Züllig et al (2020). Proteins were precipitated by adding a 3:1 volume of ice-cold acetonitrile/methanol/acetone (1/1/1, v/v/v), and samples were centrifuged at 1419 relative centrifugal force for 10 minutes (Hereaus Biofuge pico, Hanau, Germany). The resultant supernatants were aspirated into clean Eppendorf tubes and evaporated under a gentle stream of nitrogen gas at room temperature. Dry extracts were resuspended in acetonitrile/water (1/1, v/v) to 200 µl sample volume and immediately stored at −80 °C until further analysis. To evaluate data-processing and -retention times, the following mixture of metabolite standards was measured in addition to biological samples: dopamine hydrogen chloride (56610-5G; ≥98.5%), l-ornithine monohydrochloride (75469-25G; ≥99.5%), l-prolin (81710-10G; ≥99%), taurine (86330-25G; ≥99%), creatinine (C4255-10G; ≥98%), d-(+)-glucose (G8270-100G; ≥99.5%), l-alanine (A7627-1g; ≥98%), l-asparagine (A0884-25G; ≥98%), l-aspartic acid (A8949-25G; ≥99%), l-citrulline (C7629-10MG; ≥98%), l-glutamic acid (G1251-100G; ≥99%), l-glutamine (G8540-25G; ≥99%), l-histidine (H8000-5G; ≥ 99%), l-isoleucine (I2752-1G; ≥98%), l-leucine (L8000-25g; ≥98%), l-lysine (L5501-1G; ≥98%), l-methionine sulfoxide (M1126-1G), l-phenylalanine (P2126-100G;≥98%), l-serine (S4500-1G; ≥99%), l-threonine (T8625-1G;≥98%), l-tryptophan (T0254-5G; ≥98%), l-tyrosine (T3754-50G; ≥98%), l-valine (V0500-1G; ≥98%), cholic acid (C1129-25G; ≥98%), d-carnitine (544361-1G; ≥98%), decanoyl-l-carnitine (50637-10MG; ≥94%), folic acid (F7876-1G; ≥97%), hippuric acid (112003-5G; ≥98%), l-carnosine (C9625-10MG; ≥99%), palmitoyl-l-carnitine (91503-10MG; ≥95%), riboflavin (R4500-5G; ≥98%), valeryl-l-carnitine (04265-10MG; ≥95%), adenine (A8626-1G; ≥99%), cytidine (C122106-1G; ≥99%), cytosine (C3506-1G; ≥99%), d-arginine (A2646-250MG; ≥98%), choline (C7017-10MG, ≥99%), a-tocopherol (T3251-5G, ≥96%), adenosine (A9251-1G, ≥99%), and methionine (M9625-5G, ≥98%) standards were purchased from Sigma-Aldrich, and estradiol (E0950-000) was purchased from Steraloids. The final injection concentration of these standards was 10 µM desolved in acetonitrile/water (1:1, v/v).

For all samples, a full-scan mass-spectrometric interrogation of each sample's small molecule set was achieved by Dionex Ultimate 3000 ultrahigh performance liquid chromatography Orbitrap Velos Pro hybrid mass spectrometer (Thermo Fisher Scientific). Separation was performed on an Acquity UPLC BEH Amide column (2.1 × 150 mm, 1.7 µm) (Waters) and thermostated to 40 ∘C. Mobile phase A was 97% acetonitrile + 3% water + 0.1 mM ammonium formate + 0.16% formic acid. Mobile phase B was water + 0.1 mM ammonium formate + 0.16% formic acid and autosampler wash solution acetonitrile/water (1:1, v/v). The starting point of gradient elution was 5% mobile phase B and increased up to 30% over 30 minutes. Mobile phase B was reset to start conditions over a minute and re-equilibrated for 9 minutes before 2 µl of the next sample was reinjected. Flow rate was 200 µl min^{-1}, and samples were thermostatted at 8 °C in the autosampler. The Orbitrap Velos Pro operated in data-dependent acquisition mode using a HESI II ion source. Full scan spectra from m/z 60 to 1600 were acquired in the Orbitrap with a resolution of 100,000 (m/z 400) in positive mode, and the 10 most abundant ions of the full-scan spectrum were sequentially fragmented with Collision-Induced Dissociation (normalized collision energy of 50) and analyzed in the linear ion trap. Isolation width was 1.5, activation Q was 0.2, activation time was 10, and the centroided product spectra at normal scan rate were collected. The exclusion time was set to 11 seconds, and as lock mass, a polysiloxane with m/z 536.16537 was chosen. The following source parameters were used: source voltage of 4.5 kV, source temperature of 275 °C, sheath gas of 25 arbitrary units, aux gas of 8 arbitrary units, sweep gas of 0 arbitrary units, and capillary temperature of 300 °C.

Metabolite data processing was performed with Lipid Data Analyzer as described in the Lipidomics section, with the only exception being that the lipidomics target lists were substituted by a metabolomics target list containing the 40 metabolites from the retention time reference standard.

Lipidomics and metabolomics untargeted data extraction

Raw mass spectrometry data were processed on MS-DIAL software, version 4.47 (Tsugawa et al, 2020). First, mass spectrometry data (.raw) were converted to mzML format with msConvert tool (http://proteowizard.sourceforge.net). After conversion, MS-DIAL software was used for feature detection, deconvolution of spectra, peak alignment, and lipid identification (Tsugawa et al, 2019). Briefly, ionization mode (positive and negative) and data type (centroided) were selected. For peak detection process, the peak intensity threshold was set up at 1000 of amplitude, and the mass slice was set up at 0.1 Da. Linear-weighted moving average method was preferred for smoothing (smoothing level 3 scan), and minimum peak width was adjusted to 5. For deconvolution parameters, sigma window value was set up at 0.5. For alignment parameters setting, retention time and MS1 mass tolerance were selected at 0.05 minutes and 0.015 Da, respectively. Gap filling function was used for missing value interpolation. Adduct ion setting, including protonated molecule, ammonium adduct ion, and deprotonated molecule, was considered for positive and negative ion mode. For lipid species annotation, mass spectrometry finder vs 3.52 was used (Lai et al, 2018).

Lipidomics and metabolomics statistical analysis

Data visualization and statistical analysis were performed with R (version 4.2) (using the packages dplyr, openxlsx, readxl, stringr, tibble, tidyr, ggplot2, ggpubr, ggpmisc, ggrepel, ggforce, colorspace, grid, scales, missMDA, mixOmics, nlme, emmeans, rstatix) and TIBCO Spotfire (v14.3.0, TIBCO, Palo Alto, CA) (R Core Team, 2024). Absolute quantitative concentrations were obtained for 118 targeted lipids by normalizing to their internal standards. Targeted

integration of peak areas for 35 metabolites and untargeted data extraction are relative quantifications providing arbitrary units (Supplementary Data S1).

Extreme single outliers' values in untargeted features were trimmed with a MAD (median absolute deviation) score > 5, which was calculated on log_{10}-transformed data to symmetrically trim very low and very high outlier values (Leys et al, 2013). Features with >10% of all values having a MAD score > 5 were excluded from statistical analysis. Features with an intensity <100, a blank load >30%, >20% of data missing in all samples, or >70% data missing in any of the groups were also excluded. Targeted and untargeted data were combined for statistical analysis, and data were log_{10}-transformed. After transformation, all targeted metabolites and lipids as well as all untargeted features were sufficiently normally distributed and homoscedastic, according to Kolmogorov–Smirnov test and Brown–Forsythe Levene–type test, respectively. All applied statistical methods are able to provide unbiased estimates for the unbalanced group sizes and design.

The supervised multivariate PLS-DA was performed with mixOmics::plsda(…, scale = TRUE) after imputation with missMDA::imputePCA() using 6 components (Josse and Husson, 2016; Rohart et al, 2017). Significances of group differences were evaluated with mixOmics::auroc() on the basis of the first 2 components.

For univariate analysis, linear-mixed models were fitted with nlme::lme() with maximum likelihood on log_{10}-transformed data, which renders this approach nonlinear mixed models (Pinheiro and Bates, 2000, 2023). The complex design with unpaired (baseline vs healthy controls) and paired sampling (treated visits vs baseline) as well as different number of visits between patients with AD and those with DAOSD necessitated subsetting the data into different models per sample matrix (Supplementary Data S1). The use of multivariable models by including more than 1 factor (eg, time and conjunctivitis status) would have required the exclusion of unmatched groups (eg, patients without conjunctivitis or healthy controls), leading to substantial data loss and compromising the integrity of the analysis. Therefore, only the simplest models using only the factor group were tested versus models including either sex (subsets vs healthy controls) or the paired design (Patient_ID) as random factor. Model selection was based on model performance and suitability with lower Akaike information criterion (relative estimate of information loss), higher log-likelihood (goodness of fit), significance in log likelihood ratio test comparing 2 models, quality of Q–Q plots, and randomness in residual plots. The addition of the random factor (sex or Patient_ID) was found to significantly improve models for more than half of all features, whereas none reduced quality of fit. Thus, for consistency and comparability, only results from models with random factor are reported. Posthoc pairwise comparisons were readout with emmeans::emmeans(), and $P \leq .05$ was considered statistically significant. Because this was an exploratory study, all reported *P*-values were without multiple test adjustment. However, multiple test adjusted according to Benjamini–Hochberg was performed with R function stats::p.adjust() and is provided in Supplementary Data S1. Linear correlations were calculated with TIBCO Spotfire only for features and clinical or blood results with >15 numeric values (Supplementary Data S2).

Pathway analysis was performed with MetaboAnalystR 4.0 on the basis of either linear-mixed effect results or linear correlation results for both ionization modes with *P*-values as provided in Supplementary Data S1 and S2 (Pang et al, 2020). Analysis was based for each of the 7 pairwise comparisons on features with a $P < .05$ and performed with MetaboAnalystR::PerformPSEA() setting to gsea algorithm, version 2 of mummichog, 5 ppm mass tolerance, including retention time, enforcing primary ions, a minimum number of 3 metabolites per pathway, and 100 permutations against all relevant human libraries (MFN- hsa_mfn, BC - hsa_biocyc, hKE - hsa_kegg, MNL - main_nolipid_class_mset, SNL - sub_nolipid_class_mset, PRE - predicted_mset, ML - main_lipid_class_mset, SL - sub_lipid_class_mset). Three libraries' pairs (MFN - hKE, MNL - SNL, and ML - SL) partially contained 91 same pathways, so that results from the libraries SNL, SL, and hKE were not shown but are provided in Supplementary Data S1 and S2. Graphical abstract was created with BioRender.com.

ETHICS STATEMENT

This study conformed to the principles of the Declaration of Helsinki. Written informed consent was obtained from all study participants and controls. Approval was obtained from the Ethics Committee of the Medical University of Graz (ethical application number 31- 379 ex 18/19).

DATA AVAILABILITY STATEMENT

All data are available in the online Supplementary Data S1 and metabolomics mass spectrometry files at https://zenodo.org/records/11565619.

ORCIDs

Vijaykumar Patra: http://orcid.org/0000-0002-7161-7767
Natalie Bordag: http://orcid.org/0000-0002-9505-6271
Urban Cerpes: http://orcid.org/0000-0003-0704-5888
Maria Repelnig: http://orcid.org/0000-0003-3978-7659
Yohann Clement: http://orcid.org/0000-0002-9852-2856
Harald Köfeler: http://orcid.org/0000-0002-2725-9616
Andreas Wedrich: http://orcid.org/0000-0003-2533-7067
Sophie Ayciriex: http://orcid.org/0000-0003-4813-5900
Peter Wolf: http://orcid.org/0000-0001-7777-9444

CONFLICT OF INTEREST

FL received fees from AbbVie, Celgene, Eli Lilly, Galderma, Janssen-Cilag, Leo Pharma, Novartis, Pelpharma, Pfizer, and Sanofi; was a consultant at Almirall, Celgene, Eli Lilly, Galderma, Menlo Therapeutics, Novartis, Pelpharma, Pfizer, Sanofi, Trevi Therapeutics, and Vifor Pharma; was a principal investigator at Almirall, DS Biopharma, Eli Lilly, Galderma, KiniKsa, Menlo Therapeutics, Leo Pharma, Pfizer, and Trevi Therapeutics. UC received personal fees from Almirall, Mylan, and Sanofi and travel grants was ALK and Sanofi. The remaining authors state no conflict of interest.

ACKNOWLEDGMENTS

This project was financially supported by the City of Graz to VP and NW and the Dr Adele-Rabensteiner Foundation of the Austrian Association of Ophthalmology to NW and by the Austrian Science Fund FWF (W1241) to PW. The funders had no role in study design, data collection and interpretation, or the decision to submit the work for publication. We thank Dr Johannes Woltsche for his support in preparing patient characteristics table.

AUTHOR CONTRIBUTIONS

Conceptualization: VP; Data Curation: VP, NB, HK, JC, SA; Formal Analysis: NB, VP, JC, SA; Funding Acquisition: VP, NW, PW; Investigation: NW, VP, UC, DB, MR, MF, FL, AW, JH-W, PW; Methodology: HK, JC, SA, NB; Project Administration: VP; Resources: AW, JH-W, PW; Software: NB, JC, SA, VP; Supervision: VP, Validation: PW; Visualization: NB, VP, Writing – Original Draft Preparation: VP; Writing - Review and Editing: NW, NB, PW

DECLARATION OF GENERATIVE ARTIFICIAL INTELLIGENCE (AI) OR LARGE LANGUAGE MODELS (LLMs)

The authors did not use AI/LLM in any part of the research process and/or manuscript preparation.

SUPPLEMENTARY MATERIAL

Supplementary material is linked to the online version of the paper at www.jidonline.org, and at https://doi.org/10.1016/j.xjidi.2025.100361.

REFERENCES

Aguilar F, Crebelli R, Di DA, Dusemund B, Frutos MJ, Galtier P, et al. Scientific Opinion on the re-evaluation of benzoic acid (E 210), sodium benzoate (E 211), potassium benzoate (E 212) and calcium benzoate (E 213) as food additives. EFSA J 2016;14:4433.

Aydin OF, Zorlu P, Kunak B, Tezic T, Eken A. Two siblings with tyrosinaemia type 2. Eur J Pediatr 2003;162:81–3.

Boguniewicz M, Alexis AF, Beck LA, Block J, Eichenfield LF, Fonacier L, et al. Expert perspectives on management of moderate-to-severe atopic dermatitis: a multidisciplinary consensus addressing current and emerging therapies. J Allergy Clin Immunol Pract 2017;5:1519–31.

Brosnan JT, Brosnan ME. Creatine metabolism and the urea cycle. Mol Genet Metab 2010;100:S49–52.

Chari S, Clark-Loeser L, Shupack J, Washenik K. A role for leukotriene antagonists in atopic dermatitis? Am J Clin Dermatol 2001;2:1–6.

Darlenski R, Kazandjieva J, Hristakieva E, Fluhr JW. Atopic dermatitis as a systemic disease. Clin Dermatol 2014;32:409–13.

European Medicines Agency. Dupixent: EPAR - product information. https://www.ema.europa.eu/en/medicines/human/EPAR/dupixent; 2023 (accessed October 1, 2024).

Hagn G, Meier-Menches SM, Plessl-Walder G, Mitra G, Mohr T, Preindl K, et al. Plasma instead of serum avoids critical confounding of clinical metabolomics studies by platelets. J Proteome Res 2024;23:3064–75.

Hartler J, Triebl A, Ziegl A, Trötzmüller M, Rechberger GN, Zeleznik OA, et al. Deciphering lipid structures based on platform-independent decision rules. Nat Methods 2017;14:1171–4.

Hartler J, Trötzmüller M, Chitraju C, Spener F, Köfeler HC, Thallinger GG. Lipid data analyzer: unattended identification and quantitation of lipids in LC-MS data. Bioinformatics 2011;27:572–7.

Josse J, Husson F. missMDA: a package for handling missing values in multivariate data analysis. J Stat Softw 2016;70:1–31.

Kamata M, Tada Y. A literature review of real-world effectiveness and safety of dupilumab for atopic dermatitis. JID Innov 2021;1:100042.

Lai Z, Tsugawa H, Wohlgemuth G, Mehta S, Mueller M, Zheng Y, et al. Identifying metabolites by integrating metabolome databases with mass spectrometry cheminformatics. Nat Methods 2018;15:53–6.

Leys C, Ley C, Klein O, Bernard P, Licata L. Detecting outliers: do not use standard deviation around the mean, use absolute deviation around the median. J Exp Soc Psychol 2013;49:764–6.

Liebisch G, Vizcaíno JA, Köfeler H, Trötzmüller M, Griffiths WJ, Schmitz G, et al. Shorthand notation for lipid structures derived from mass spectrometry. J Lipid Res 2013;54:1523–30.

Matyash V, Liebisch G, Kurzchalia TV, Shevchenko A, Schwudke D. Lipid extraction by methyl-tert-butyl ether for high-throughput lipidomics. J Lipid Res 2008;49:1137–46.

Maudinet A, Law-Koune S, Duretz C, Lasek A, Modiano P, Tran THC. Ocular surface diseases induced by dupilumab in severe atopic dermatitis. Ophthalmol Ther 2019;8:485–90.

Meijer F, Van Delft JL, Garrelds IM, Van Haeringen NJ, Kijlstra A. Nitric oxide plays a role as a mediator of conjunctival edema in experimental allergic conjunctivitis. Exp Eye Res 1996;62:359–65.

Navarro MN, Gómez de las Heras MM, Mittelbrunn M. Nicotinamide adenine dinucleotide metabolism in the immune response, autoimmunity and inflammageing. Br J Pharmacol 2022;179:1839–56.

Pang Z, Chong J, Li S, Xia J. MetaboAnalystR 3.0: toward an optimized workflow for global metabolomics. Metabolites 2020;10:186.

Patra V, Woltsche N, Cerpes U, Bokanovic D, Repelnig M, Joshi A, et al. Persistent neutrophil infiltration and unique ocular surface microbiome typify dupilumab-associated conjunctivitis in patients with atopic dermatitis. Ophthalmol Sci 2023;0:100340.

Phylactou M, Jabbour S, Ahmad S, Vasquez-Perez A. Corneal perforation in patients under treatment with dupilumab for atopic dermatitis. Cornea 2022;41:981–5.

Pinheiro JC, Bates DM. Mixed-Effects Models in S and S-PLUS. New York: Springer; 2000.

Pinheiro J, Bates D, R Core Team. nlme: Linear and Nonlinear Mixed Effects Models. R package version 3.1-164. 2023. https://CRAN.R-project.org/package=nlme. (accessed October 29, 2024).

R Core Team. _R: A Language and Environment for Statistical Computing_. Vienna, Austria: R Foundation for Statistical Computing; 2024. https://www.R-project.org/. (accessed October 29, 2024).

Rohart F, Gautier B, Singh A, Lê Cao KA. mixOmics: an R package for 'omics feature selection and multiple data integration. PLoS Comput Biol 2017;13:e1005752.

Serhan CN, Chiang N, Van Dyke TE. Resolving inflammation: dual anti-inflammatory and pro-resolution lipid mediators. Nat Rev Immunol 2008;8:349–61.

Song X, Liang Y, Zhou S, Xie W, Yang Q, Ma N, et al. Glutamine alleviates Lipopolysaccharide-induced corneal epithelial inflammation and oxidative stress in dogs. Exp Eye Res 2023;234:109607.

Ständer S. Atopic dermatitis. N Engl J Med 2021;384:1136–43.

Thormann K, Lüthi AS, Deniau F, Heider A, Cazzaniga S, Radonjic-Hoesli S, et al. Dupilumab-associated ocular surface disease is characterized by a shift from Th2/Th17 toward Th1/Th17 inflammation. Allergy 2024;79:937–48.

Triebl A, Trötzmüller M, Hartler J, Stojakovic T, Köfeler HC. Lipidomics by ultrahigh performance liquid chromatography-high resolution mass spectrometry and its application to complex biological samples. J Chromatogr B Analyt Technol Biomed Life Sci 2017;1053:72–80.

Tsugawa H, Ikeda K, Takahashi M, Satoh A, Mori Y, Uchino H, et al. A lipidome atlas in MS-DIAL 4. Nat Biotechnol 2020;38:1159–63.

Tsugawa H, Nakabayashi R, Mori T, Yamada Y, Takahashi M, Rai A, et al. A cheminformatics approach to characterize metabolomes in stable-isotope-labeled organisms. Nat Methods 2019;16:295–8.

Utine CA, Li G, Asbell P, Pflugfelder S, Akpek E. Ocular surface disease associated with dupilumab treatment for atopic diseases. Ocul Surf 2021;19:151–6.

Weidinger S, Novak N. Atopic dermatitis. Lancet 2016;387:1109–22.

Yu Z, Kastenmüller G, He Y, Belcredi P, Möller G, Prehn C, et al. Differences between human plasma and serum metabolite profiles. PLoS One 2011;6:e21230.

Zandl-Lang M, Züllig T, Trötzmüller M, Naegelin Y, Abela L, Wilken B, et al. Changes in the cerebrospinal fluid and plasma lipidome in patients with Rett syndrome. Metabolites 2022;12:291.

Zhang L, Wen X, Hou Y, Yang Y, Song W, Zeng Y, et al. Integrated metabolomics and lipidomics study of patients with atopic dermatitis in response to dupilumab. Front Immunol 2022;13:1002536.

Zhang L, Zeng Y, Sun J. Progress of metabolomics in atopic dermatitis: a systematic review. J Dtsch Dermatol Ges 2023;21:229–36.

Zhang Y, Dijkman PM, Zou R, Zandl-Lang M, Sanchez RM, Eckhardt-Strelau L, et al. Asymmetric opening of the homopentameric 5-HT3A serotonin receptor in lipid bilayers. Nat Commun 2021;12:1074.

Zhu X, Wei L, Rong X, Zhang Y, Zhang Q, Wen X, et al. Conjunctival microbiota in patients with type 2 diabetes mellitus and influences of perioperative use of topical levofloxacin in ocular surgery. Front Med (Lausanne) 2021;8:605639.

Zou X, Huang H, Tan Y. Genetically determined metabolites in allergic conjunctivitis: a Mendelian randomization study. World Allergy Organ J 2024;17:100894.

Züllig T, Zandl-Lang M, Trötzmüller M, Hartler J, Plecko B, Köfeler HC. A metabolomics workflow for analyzing complex biological samples using a combined method of untargeted and target-list based approaches. Metabolites 2020;10:342.

Zysset-Burri DC, Schlegel I, Lincke JB, Jaggi D, Keller I, Heller M, et al. Understanding the Interactions between the ocular surface microbiome and the tear proteome. Invest Ophthalmol Vis Sci 2021;62:8.